BRAND PROPAGATION FROM LARGE-SCALE FIRES

John P. Woycheese, Patrick J. Pagni, and Dorian Liepmann
Department of Mechanical Engineering
University of California
Berkeley, CA 94720-1740

ABSTRACT

This paper is one of a series on brand lofting and propagation. Here, spherical brand propagation in a constant ambient wind is addressed. Maximum propagation distances are calculated for wooden brands with diameters up to 0.18 m, which are lofted above axisymmetric pool fires with heat release rates, $\dot{Q}_o$, between 1 MW and 3 GW. Winds of 1.8 m/s $\leq U_w \leq$ 92 m/s are considered. A maximum propagation distance equation is developed as a function of $\dot{Q}_o$, U_w and wood type, or β. Cedar brands (β = 1), lofted by fires with $\dot{Q}_o$ = 1 MW, 50 MW and 1 GW, travel a maximum of 49 m, 290 m and 1100 m, respectively, in 10 m/s winds before landing at burn out. Brands between a "collapse" diameter, $d_{col} = 0.49\ \dot{Q}_o^{0.269}\ \beta^{0.782}$, and a maximum loftable diameter, $d_{o,max} = 0.454\ \beta\ \dot{Q}_o^{0.04}$, propagate the same maximum distance, since the larger brands move slower and therefore have more time to combust. Hence, only brands with $0 \leq d \leq d_{col}$ need be studied for given $\dot{Q}_o$, U_w and β.

INTRODUCTION

Spot ignition by burning brands far ahead of the flame front of large fires is an important mechanism for fire spread in post-earthquake and urban/wildland intermix fires[1]. The 20 October 1991 Oakland Hills Fire quickly overwhelmed fire-fighting efforts, in part due to the propagation of flaming brands hundreds of meters ahead of the fire front.[1] Brand propagation from large fires is a complex problem. Important issues include time-dependent wind and plume velocity fields, brand size and shape distributions and combustion rates, and terrain effects. Although spotting has received considerable attention in the forest fire community,[2-5] little research quantifies brand transport from burning structures. This paper provides maximum propagation distances for spherical brands lofted from large, single-plume fires above burning structures. Ambient wind, the propagation medium, is assumed to be constant and horizontal and the terrain is assumed flat. Equations for the upper limit of brand sizes and propagation distances are determined as functions of heat release rate, wind velocity, and brand and air properties. This is a companion paper to the authors' previous article[6] on brand lofting, which appeared in the Proceedings of the 2nd International Conference on Fire Research and Engineering (ICFRE2). Previous studies by Tarifa, et al.,[7,8] and Lee, et al.,[9,10] assume a constant vertical velocity for lofting calculations with particles released at arbitrary heights. A more accurate axisymmetric pool fire plume flow field[11] has been used to determine the optimum lofting height for downwind propagation.[6] The limitations in brand shape enable comparison to the literature;[7,8] subsequent work will explore multi-dimensional shapes and large-eddy-simulation plume models. This paper is divided into four sections: Analysis, Results, Numerical Examples and Conclusions. In Analysis, the lofting, combustion and propagation equations are developed from a brand momentum balance. Dimensionless Results of these equations are presented in the next section. Numerical Examples provides both curve fits of the predictions and dimensional calculations for representative fire cases. The Conclusions section summarizes the results and suggests future work.

ANALYSIS

Force Balance

Conservation of brand momentum[12] is

$$\frac{d}{dt}(m\mathbf{V}) = \sum_i \mathbf{F}_i \qquad (1)$$

where $\mathbf{V}$ is the particle velocity with respect to ground, $\mathbf{F}_i$ are the forces on the particle, and m

is the mass. A spherical body in a velocity field is affected by two forces: drag and gravity. The gravity force is

$$\mathbf{F}_g = -mg\hat{\mathbf{k}} \tag{2}$$

where g is the acceleration due to gravity and $\hat{\mathbf{k}}$ indicates that the force acts in the vertical direction. The drag force is

$$\mathbf{F}_d = \frac{1}{2}\rho_a A_c C_d |\mathbf{W}|^2 \frac{\mathbf{W}}{|\mathbf{W}|} \tag{3}$$

where A_c is the cross-sectional area of the brand, ρ_a is the density of air, C_d is the drag coefficient, and $\mathbf{W}$ is the velocity of the flow relative to the particle, $\mathbf{W} \equiv \mathbf{U} - \mathbf{V}$. The drag force acts in the direction of $\mathbf{W}$ with a strength proportional to the square of $|\mathbf{W}|$. With the above, in cartesian coordinates, Eq. (1) becomes a 3-D extension from previous analyses:[6]

$$\frac{d}{dt}(mV_x) = \frac{1}{2}\rho_a A_c C_d |\mathbf{W}| W_x \quad \text{(a)}$$

$$\frac{d}{dt}(mV_y) = \frac{1}{2}\rho_a A_c C_d |\mathbf{W}| W_y \quad \text{(b)}$$

$$\frac{d}{dt}(mV_z) = \frac{1}{2}\rho_a A_c C_d |\mathbf{W}| W_z - mg \quad \text{(c)} \tag{4}$$

In Eq. (4), the change in momentum for the z-direction offsets the drag and gravity forces; momentum change balances drag in the horizontal plane. If the prevailing winds are assumed to be steady and irrotational, prudent selection of axes reduces the problem to two dimensions in x and z. Schematics of the brand, coordinates and forces can be found in Fig. 1.

With time-dependent particle mass and velocity, the particle acceleration is

$$\frac{dV_x}{dt} = \frac{1}{2}\left(\frac{\rho_a A_c C_d}{m}\right)\mathbf{W}|W_x - \left(\frac{V_x}{m}\right)\frac{dm}{dt} \quad \text{(a)}$$

$$\frac{dV_z}{dt} = \frac{1}{2}\left(\frac{\rho_a A_c C_d}{m}\right)\mathbf{W}|W_z - \left(\frac{V_z}{m}\right)\frac{dm}{dt} - g \quad \text{(b)} \tag{5}$$

with the wind acting in the x-direction. In this study, the brands are modeled as spheres to employ the available literature for both C_d and temporal size change. The mass and cross-sectional area of a sphere, $m = (\pi d^3\rho_s)/6$ and $A_c = (\pi d^2)/4$, are introduced into Eq. (5), where ρ_s is the homogenized density of the particle and d its diameter. The accelerations become

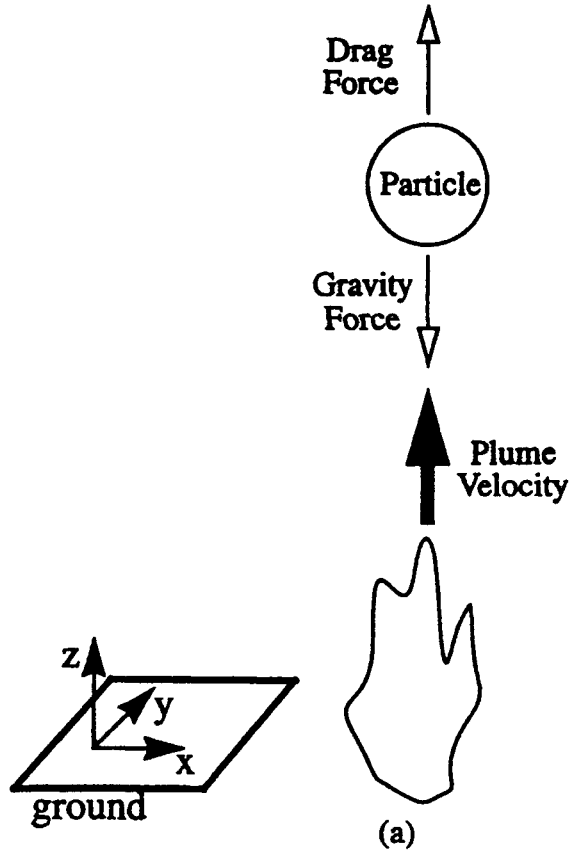

Figure 1a. Force balance on a brand in a velocity field along the plume centerline, where horizontal velocities are assumed to be zero.

$$\frac{dV_x}{dt} = \frac{3}{4}\left(\frac{\rho_a}{\rho_s}\right)\left(\frac{C_d}{d}\right)|\mathbf{W}|W_x - \left(\frac{3V_x}{d}\right)\frac{dd}{dt} \quad \text{(a)}$$

$$\frac{dV_z}{dt} = \frac{3}{4}\left(\frac{\rho_a}{\rho_s}\right)\left(\frac{C_d}{d}\right)|\mathbf{W}|W_z - \left(\frac{3V_z}{d}\right)\frac{dd}{dt} - g \quad \text{(b)} \tag{6}$$

The first term on the right-hand side of Eq. (6) is the acceleration of the particle due to drag. The second term expresses the acceleration from the change in particle mass with respect to time ($dd/dt < 0$), assuming constant brand density. The additional term in the z-direction accounts for deceleration due to gravity.

Velocity Field

Several models quantify the fire plume velocity field,[11,13-16] each applicable to different conditions. This study uses a slightly modified version of the Baum and McCaffrey plume model.[6,11,13] In this

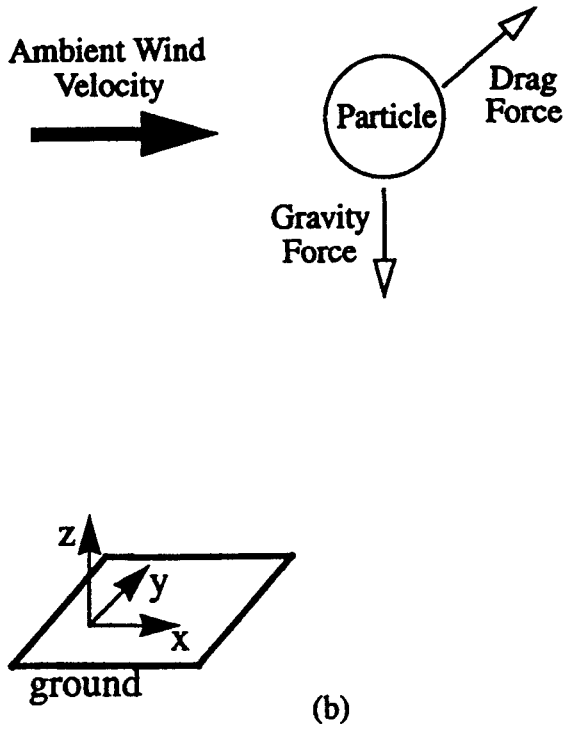

Figure 1b. Force balance on a brand in a constant ambient wind acting along the x-axis only.

model, the plume is divided into three vertical sections, corresponding to burning, intermittent flame and plume zones. The centerline velocity is

$$U_p^* = 2.13(z^*)^{1/2} \qquad z^* \le 1.32 \qquad (a)$$
$$U_p^* = 2.45 \qquad 1.32 < z^* \le 3.3 \qquad (b)$$
$$U_p^* = 3.64(z^*)^{-1/3} \qquad z^* > 3.3 \qquad (c) \qquad (7)$$

where $U_p^* = U_p / U_c$, $z^* = z/z_c$, and

$$U_c = \left(\frac{\dot{Q}_o g^2}{\rho_a c_p T_o}\right)^{1/5} \qquad (a)$$

$$z_c = \left(\frac{\dot{Q}_c}{\rho_a c_p T_o \sqrt{g}}\right)^{2/5} \qquad (b) \qquad (8)$$

$\dot{Q}_o$ is the rate of heat release for the fire and ρ_a, c_p and T_o are the ambient density, specific heat and temperature. With zero initial brand velocity, the lofting problem collapses to one dimension in z. The relative velocity within the plume is

$$W_x = -V_x = 0 \qquad (a)$$
$$W_z = U_p - V_z \qquad (b) \qquad (9)$$

For this paper, the brand follows the (assumed vertical) plume centerline velocity in the lofting phase,[6,13] and is removed from the plume at that height which results in maximum propagation – removal at greater heights results in burnout above the ground and at lower heights in smaller propagation distances – to be immersed in the horizontal velocity field of the ambient wind. After the brand is removed from the plume, it is subjected to a horizontal velocity field. The ambient wind near a fire varies greatly depending on terrain, time of fire, and atmospheric conditions. In general, wind is a function of height and time.[6,7,17] To provide limiting cases for the propagation of burning brands, a high-velocity, constant, horizontal wind is used for this study. Tarifa, et al.[7,8] used this approach "for simplicity, and because of the lack of actual data." The relative velocities outside of the plume are

$$W_x = U_w - V_x \qquad (a)$$
$$W_z = -V_z \qquad (b) \qquad (10)$$

where U_w is the constant velocity of the ambient wind.

Supplementary Models

The burning-droplet problem models a spherical fuel particle combusting in an oxidizing, quiescent atmosphere and can be adopted as a crude first approximation for wooden brands. This model is the most realistic of the three used in previous work[6] and it exploits spherical symmetry. Future work with various brand shapes will examine the complete set of aerodynamic forces and will incorporate forced convection effects on the combustion rate. A companion program is underway to quantify brand combustion rates in a low-speed combustion wind tunnel for a wide variety of brand shapes. The diameter regression rate from droplet burning is an underestimate because of the effects of forced convection.

In keeping with experimental data (e.g., Tarifa, et al.[7,8]), the wood is assumed to be a homogeneous solid. In addition, it is assumed that the brand's relative velocity is sufficient to remove ash from surface combustion and that the radiative and convective heat losses balance with the energy generation provided by combustion. Brands that extinguish when these assumptions do not hold do not present a spotting risk. Adjust-

ment of B or ρ_s may account for a small layer of ash. The regression rate of the spherical brand diameter is

$$\frac{dd}{dt} = -4\alpha\left(\frac{\rho_a}{\rho_s}\right)\left(\frac{\ln(1+B)}{d}\right) \tag{11}$$

where α is the thermal diffusivity of air and B is the mass transfer number for wood, here assumed to be 1.2.[6]

The drag coefficient, C_d, primarily depends upon Reynolds Number and body shape. There are numerous equations in the literature correlating $C_d(Re)$ for spheres near terminal velocity;[18-21] that of Haider and Levenspiel[21] is accurate for $Re < 2.6 \times 10^5$. Examination of the drag coefficient[6] reveals that a constant may suffice for spherical bodies. $C_d = 0.45$ is accurate to within five percent for $1.2 \times 10^4 < Re < 2.6 \times 10^5$ and will be adopted throughout this paper.

Initial Conditions

The problem has five dependent variables, V_z, V_x, d, x and z and one independent variable, t. U_p is a function of z, from Eq. (7), and thus is not a separate dependent variable; U_w is assumed constant. The velocity, acceleration and propagation distance of the brand are assumed to be zero at $t = 0$ and the density and diameter of the brand are known initially; only the initial height is not known *a priori.*

For each initial diameter, d_o, there is a unique initial height, z_o, in the Baum-McCaffrey plume model below which the brand will sink because the gravity force exceeds drag. Brands and non-combusting particles are lofted at the heights at which the wind velocity exceeds their terminal velocity. With the brand and wind velocities initially zero, $\mathbf{W} = U_p\hat{\mathbf{k}}$, which is always positive. Equation (6), at $t = 0$, reduces to

$$0 = \frac{3}{4}\left(\frac{\rho_a}{\rho_s}\right)\left(\frac{C_d}{d}\right)U_p^2 - g, \tag{12}$$

where $dV_z/dt = 0$ is an initial condition. Equation (12) identifies the minimum height at which the plume can support a spherical particle of a given diameter. Substituting for the fire plume centerline velocity, $U_p = 2.13\ U_c\ (z_o/z_c)^{1/2}$, and solving for z_o gives the initial brand height as

$$z_o = \left(\frac{1}{2.13}\right)^2\left(\frac{z_c}{U_c^2}\right)\left(\frac{4}{3}\right)\left(\frac{dg}{C_d}\right)\left(\frac{\rho_s}{\rho_a}\right). \tag{13}$$

Solving Eq. (12) for d when the plume velocity is maximized ($U_p = 2.45U_c$) gives the maximum loftable diameter,

$$d_{o,max} = \frac{3}{4}\left(\frac{\rho_a}{\rho_s}\right)\left(\frac{C_d}{g}\right)(2.45U_c)^2. \tag{14}$$

Non-Dimensionalization

Maximum information, in terms of a minimum number of parameters, is extracted from equations that are dimensionless with respect to the appropriate characteristic quantities for each variable.[22] The equations to be non-dimensionalized are

$$\frac{dV_x}{dt} = \frac{3}{4}\left(\frac{\rho_a}{\rho_s}\right)\left(\frac{C_c}{d}\right)|\mathbf{U} - \mathbf{V}|(U_w - V_x) - \left(\frac{3V_x}{d}\right)\frac{dd}{dt} \quad (a)$$

$$\frac{dV_z}{dt} = \frac{3}{4}\left(\frac{\rho_a}{\rho_s}\right)\left(\frac{C_d}{d}\right)|\mathbf{U} - \mathbf{V}|(U_p - V_z) - \left(\frac{3V_z}{d}\right)\frac{dd}{dt} - g \quad (b)$$

$$\frac{dx}{dt} = V_x \quad (c)$$

$$\frac{dz}{dt} = V_z \quad (d) \tag{15}$$

with dd/dt given by Eq. (11). Note that $d\rho_s/dt = 0$ is assumed. The boundary conditions are $\mathbf{V}(t=0) = 0, d(0) = d_o, z(0) = z_o = (1/2.13)^2(z_c/U_c^2)(4/3)(dg/C_d)(\rho_s/\rho_a)$ and $x(0) = 0$. The dimensionless variables are defined as

$$\mathbf{V}^* = \frac{\mathbf{V}}{U_c}\ \mathbf{W}^* = \frac{\mathbf{W}}{U_c}\ U_p^* = \frac{U_p}{U_c}\ U_w^* = \frac{U_w}{U_c}$$

$$z^* = \frac{z}{z_c}\quad x^* = \frac{x}{z_c}\quad D^* = \frac{d}{D_c}\quad t^* = \frac{t}{t_c} \tag{16}$$

where U_c and z_c are defined by Eq. (8), $t_c = z_c/U_c$, $x_c = U_c t_c = z_c$, and $C_d = 0.45$. D_c remains to be determined.

Substituting Eqs. (16) into Eqs. (15a and b) gives

$$\frac{dV_x^*}{dt^*} = \frac{3}{4}\left(\frac{\rho_a}{\rho_s}\right)\left(\frac{C_d}{D^*}\right)\left(\frac{t_c U_c}{D_c}\right)|\mathbf{W}^*|W_x^* - \left(\frac{3V_x^*}{D^*}\right)\frac{dD^*}{dt^*} \quad (a)$$

$$\frac{dV_z^*}{dt^*} = \frac{3}{4}\left(\frac{\rho_a}{\rho_s}\right)\left(\frac{C_d}{D^*}\right)\left(\frac{t_c U_c}{D_c}\right)|\mathbf{W}^*|W_z^* - \left(\frac{3V_z^*}{D^*}\right)\frac{dD^*}{dt^*} \quad (b) \tag{17}$$

from which the characteristic diameter is

$$D_c = \frac{3}{4}\left(\frac{\rho_a}{\rho_s}\right)(C_d t_c U_c) = \left(\frac{3C_d}{4}\right)\left(\frac{\rho_a}{\rho_s}\right)\left(\frac{\dot{Q}_o}{\rho_a c_p T_o\sqrt{g}}\right)^{2/5} \tag{18}$$

(This characteristic diameter is equal to $(3C_d d_c)/(4\rho^*)$ in Ref. 6.) The dimensionless brand acceleration equations become

$$\frac{dV_x^*}{dt^*} = \frac{|\mathbf{W}^*|W_x^*}{D^*} - \left(\frac{3V_x^*}{D^*}\right)\frac{dD^*}{dt^*} \quad \text{(a)}$$

$$\frac{dV_z^*}{dt^*} = \frac{|\mathbf{W}^*|W_z^*}{D^*} - \left(\frac{3V_z^*}{D^*}\right)\frac{dD^*}{dt^*} - 1 \quad \text{(b)} \qquad (19)$$

The dimensionless brand diameter regression rate, from Eq. (11), is

$$\frac{dD^*}{dt^*} = -\frac{1}{\Phi D^*} \qquad (20)$$

where

$$\Phi = \left(\frac{9}{64}\right)\left(\frac{\rho_a}{\rho_s}\right)\left(\frac{C_d^2}{\alpha \ln(1+B)}\right)\left(\frac{\dot{Q}_o\sqrt[3]{g}}{\rho_a c_p T_o}\right)^{3/5} \qquad (21)$$

is a burning parameter based on the droplet-burning equation. Φ absorbs the fire size and wood and air properties for the diameter regression rate. The equations for height and distance, from Eqs. (15c and d) become

$$\frac{dx^*}{dt^*} = V_x^* \quad \text{(a)}$$

$$\frac{dz^*}{dt^*} = V_z^* \quad \text{(b)} \qquad (22)$$

Equations (19, 20, and 22) must be solved simultaneously, where W^* is

$$W_x^* = U_p^* - V_z^* \qquad (23)$$

in the plume and

$$W_z^* = U_w^* - V_x^* \quad \text{(a)}$$

$$W_z^* = -V_z^* \quad \text{(b)} \qquad (24)$$

for propagation. The dimensionless initial conditions are $V_x^*(0) = V_z^*(0) = 0$, $z^*(0) = z_o^*$, $x^*(0) = 0$, and $D^*(0) = D_o^*$, where $z_o^* = 0.22D_o^*$ from Eq. (13). The maximum loftable diameter, from Eq. (14), is $D_{o,max}^* = 6$.

The terminal velocity of brands larger than $D_{o,max}^*$ is greater than the maximum plume velocity. These brands will fall either to the ground or until they meet three conditions: $D^* \le D_{o,max}^*$, $z^* \ge 0.22D^*$, and $V^* = 0$. The former case poses no spotting risk. The latter mirrors the initial conditions for the brands of this study – the slight variations do not lead to appreciable differences in lofting height[6] – and thus no new information is gathered. Characteristic quantities for a range of heat release rates can be found in Table 1.

RESULTS

The propagation results for spherical, combusting brands with burning-droplet regression rates are presented in this section. Details of the lofting calculations for combusting brands can be found in Ref. 6. Lofted particles are removed from the plume at the height (as shown here in Figs. 4a and 4b) that maximizes the spotting distance. Brands released from greater heights completely combust in the air, with no spotting risk; lower heights result in shorter propagation distances.

The dimensionless regression rate depends inversely on both the dimensionless diameter, D^*, and the dimensionless burning parameter, Φ; thus, the diameter decreases faster the smaller the diameter. The temporal decrease in brand diameter during the propagation phase is shown in Fig. 2, parameterized in the initial dimensionless diameter, D_o^*, for $\Phi = 200$, and in Fig. 3, parameterized in Φ for $D_o^* = 5$. At removal from plume, the brand size for maximum propagation is inversely related to Φ for a given initial brand size and wind velocity. Brands with larger Φ propagate farther due to their lower diameter regression rate.

For sufficiently large brands during lofting, the acceleration equation,

$$\frac{dV_z^*}{dt^*} = \frac{U_p^* - V_z^*}{D^*} + \frac{3V_x^*}{\Phi D^{*2}} - 1 \qquad (25)$$

is dominated by the drag and gravity terms (the first and third terms on the right-hand side of Eq. (25)). The brand velocity and acceleration decrease (when the brand enters the thermal plume zone as shown in Figs. 12 and 15 of Ref. 6) until these two terms are nearly in balance.

Table 1. Example Values of Characteristic Quantities

				For cedar with ρ_s = 315 kg/m^3 and B = 1.2	
$\dot{Q}_o$ (MW)	U_c (m/s)	z_c (m)	t_c (s)	D_c (mm)	ϕ
1	3.1	0.96	0.31	1.2	17
50	6.7	4.6	0.69	5.7	180
1000	12	15	1.2	19	1100
3000	15	24	1.6	29	2100

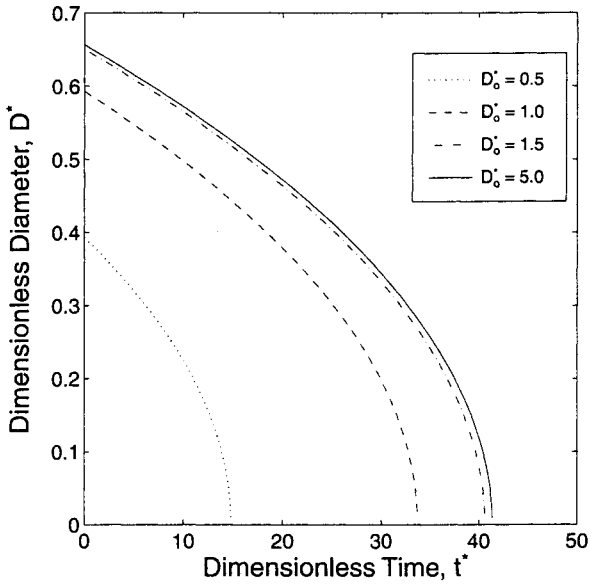

Figure 2. Dimensionless diameter as a function of dimensionless time; Φ = 200 and D_o^* as noted.

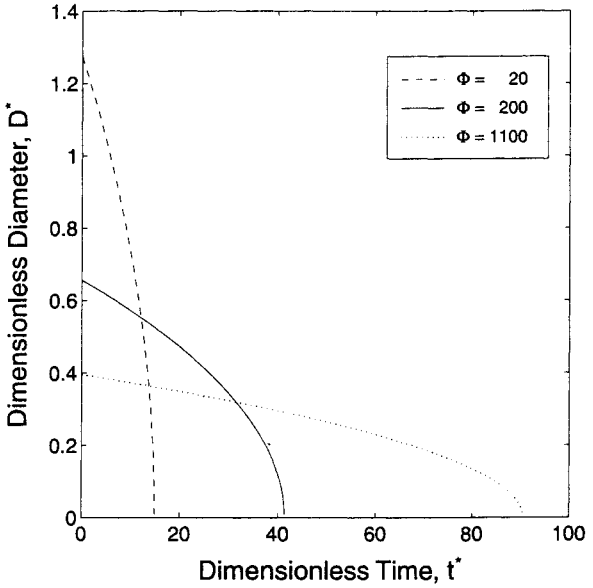

Figure 3. Dimensionless diameter as a function of dimensionless time; D_o^* = 5 and Φ as noted.

As the brand size decreases, the middle term in Eq. (25) becomes significant. This combustion acceleration acts with the drag term to increase the brand acceleration, overcoming the gravity term. The diameter at which this effect occurs is usually smaller than the diameter at which the brand is ejected from the plume for maximum propagation.

An interesting result from these calculations is the existence of similarity for large brands, i.e. those greater than some critical collapse diameter, D_{col}^*. All brands with $D_o^* < D_{col}^*$ have the same maximum lofting height and the same propagation distance because they burn down to the same size at the same height at some point during their lofting history. Once two brands have the same diameter and height at any one point, they are identical at all future times. The larger brands rise more slowly and therefore have more time to combust. This results in the plateau shown in Figs. 4a and 4b. Figure 4a shows the maximum lofting height, $z_{max,loft}^*$, as a function of D_o^* and Φ. The curves can be fit to within an average 10% by the expression

$$z_{max,loft}^* = 5.15\Phi^{0.36}(\tanh(0.62D_o^*\Phi^{0.22} - 1) + 0.76) \quad (26)$$

A similar plateau can be seen in Fig. 4b, where the maximum propagation diameter is shown as a function of D_o^* and Φ. These curves are also fit by

$$z_{max,prop}^* = 2.82\Phi^{0.39}(\tanh(0.74D_o^*\Phi^{0.22} - 2) + 0.96) \quad (27)$$

to within an average 15%, where the tanh function is suggested by the large D_o^* similarity. The brands are ejected from the plume at the height that enables the brand to travel the farthest distance while still landing with a mass approaching zero. Thus, the curve for $z_{max,prop}^*$ will follow that for $z_{max,loft}^*$.

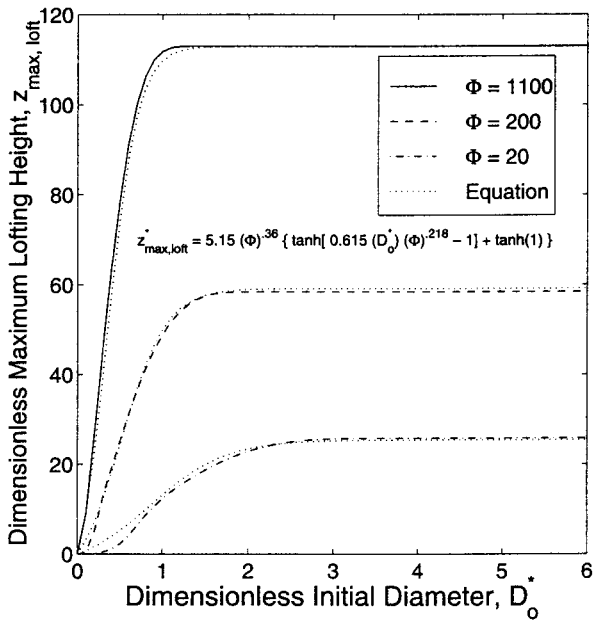

Figure 4a. The maximum loftable height as a function of initial dimensionless diameter is constant for $D^*_o < D^*_o$. The brands that satisfy this condition all have the same maximum altitude for a given Φ.

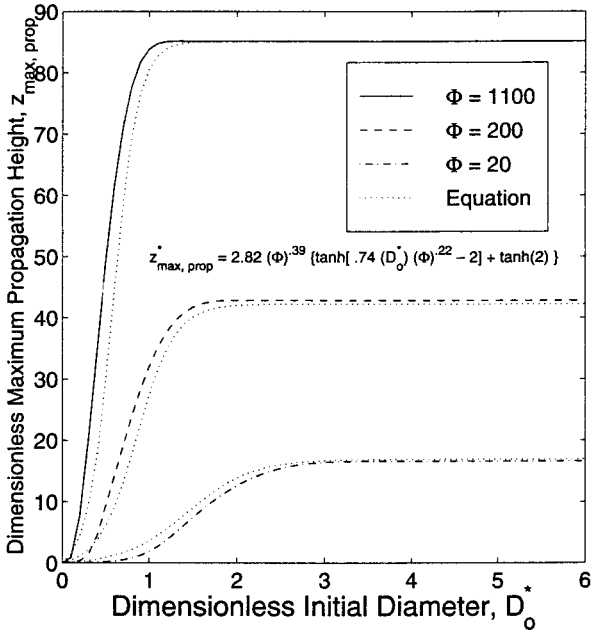

Figure 4b. The maximum propagation height as a function of initial dimensionless diameter is constant for $D^*_o > D^*_o$. The brands that satisfy this condition have the maximum propagation range for a given Φ.

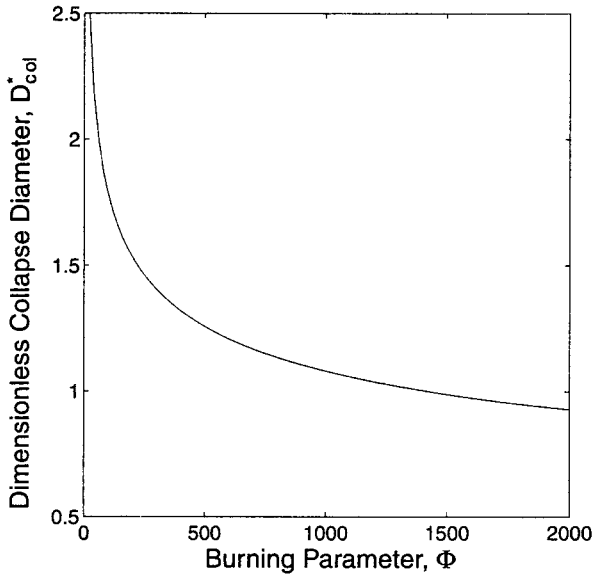

Figure 5. Dimensionless collapse diameter as a function of Φ. Spherical particles with initial dimensionless diameters greater than the collapse diameter for a given Φ propagate no farther than a sphere with D^*_{col}, given the same Φ, U^*_w, and initial conditions (except diameter).

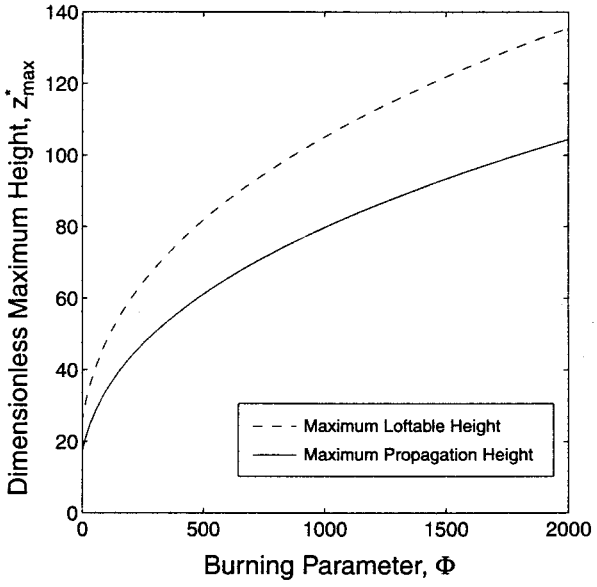

Figure 6. The maximum loftable height with respect to Φ is given by the dashed line. The maximum propagation height with respect to Φ is given by the solid line. The loftable height is independent of ambient wind, and the propagation height varies with wind speed by less than 7% over the range $0 \le U^*_w \le 6$.

The collapse diameter is an inverse function of Φ, as shown in Fig. 5. The brand regression rate is likewise an inverse function of Φ; this influences brand lifetime, as shown in Fig. 3. Brands with larger Φ combust slower, and thus can be of smaller size before they must propagate to return to ground with finite size; thus, a larger Φ corresponds to a smaller D^*_{col}.

Figure 6 provides the upper limit for loftable and propagation heights as functions of Φ. The

increase in height with Φ approaches the 2/5th power; this would indicate a dependence on fire size approximately to the 1/4th power.

The maximum loftable height for a given brand is independent of ambient wind due to the assumed independence of the lofting and propagation velocity fields. The maximum propagation height, however, varies slightly with wind speed for a particular particle due to the dependence of drag on **W**. This variation is less than 7% over the range studied ($0.3 \leq U_w^* \leq 6$).

The brand height as it propagates downwind is shown in Fig. 7, parameterized in D_0^* for $\Phi = 200$ and $U_w^* = 3$. A brand with $D_0^* = 1.5$ has a maximum propagation distance only slightly less than a brand with $D_0^* = 5$ (D_{col}^* for $\Phi = 200$). Fig. 8 gives the same information, but parameterized in Φ for $D_0^* = 5$ and $U_w^* = 3$. Fig. 9 shows the ratio of dimensionless propagation distance to horizontal wind as a function of burning parameter, parameterized in $U_w^* = 0.3$, 0.6 and 6. For $U_w^* > 3$, these plots approach a single curve.

This study, unlike previous work,[6,13] assumes that the $C_d = 0.45$ for a sphere, rather than a function of Reynolds number. This assumption is valid within 5% for $1.2 \times 10^4 < Re < 2.6 \times 10^5$, where $Re = (d\,|\mathbf{W}|)/\nu$. As a brand burns up, however, $Re \to 0$, so that the calculations using a constant C_d for all Re must be assessed. A comparison of the propagation path for identical brands introduced into the two models ($C_d = 0.45$ and $C_d = C_d(Re)$) is given in Fig. 10. For $\Phi = 200$, the Reynolds number ranges from 2×10^4 to 0 over the life of the brands in this figure. (For $\Phi = 1100$, $0 < Re < 1.2 \times 10^5$ for the same initial dimensionless brand size). Note that the brand

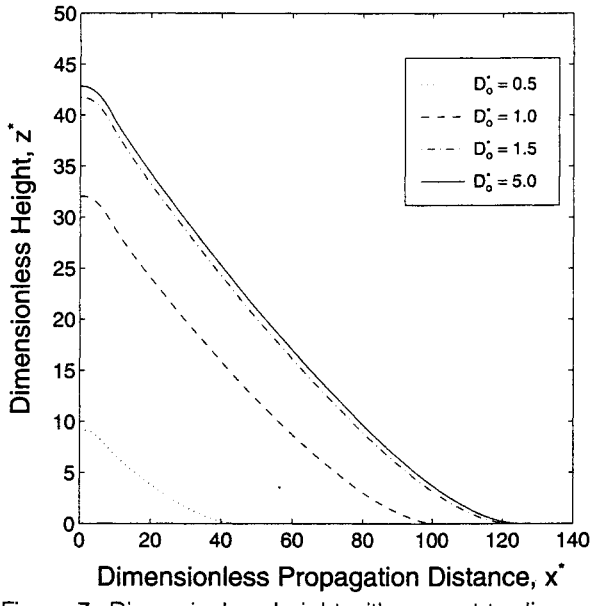

Figure 7. Dimensionless height with respect to dimensionless propagation distance for $\Phi = 200$, $U_w^* = 3$, and D_o^* as noted.

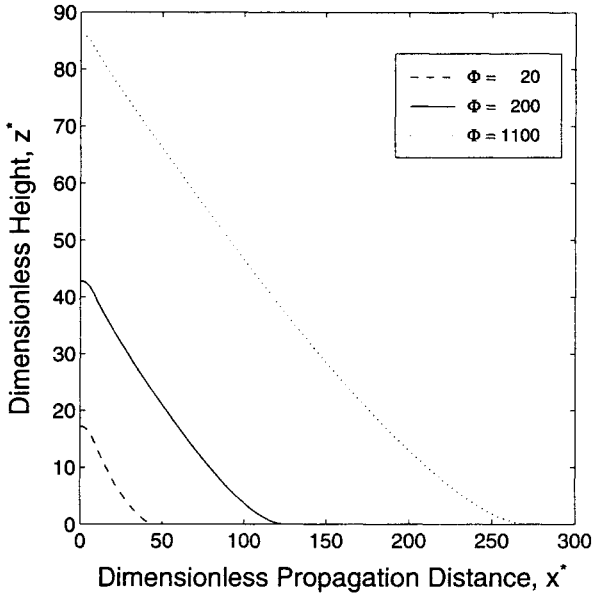

Figure 8. Dimensionless height with respect to dimensionless propagation distance for $U_w^* = 3$, $D_o^* = 5$, and Φ as noted.

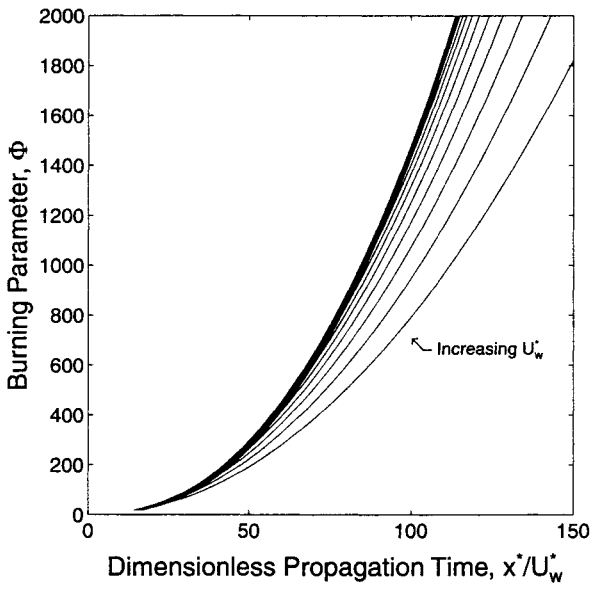

Figure 9. Dimensionless propagation time as a function of Φ, where $U_w^* = 0.3, 0.6, \ldots, 6$. The curves collapse for U_w^*.

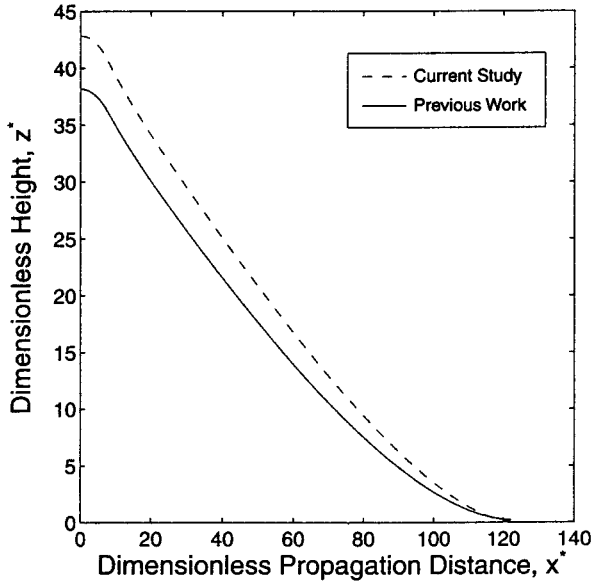

Figure 10. Dimensionless height as a function of dimensionless propagation distance for $U_w^* = 3$. The dashed line indicates current study ($C_d = 0.45$, $D_o^* = 3.9$, $\Phi = 200$); the solid line illustrates previous work[6,13] ($C_d(Re)$, $d_o^* = 10000$, $\rho^* = 1/7600$, $B = 1.2$, $Pr = 0.7$).

for the current study exits the plume at a greater height, but travels the same distance. The drag coefficient, and, therefore, drag, in the previous study is smaller prior to propagation initiation, which results in a lower initial propagation height. This coefficient increases as the Reynolds number decreases with diameter, so that the drag force increases with respect to the current study as the brand combusts.

Numerical Examples

This section addresses the professional needs of the practicing engineer by providing dimensional numerical examples of typical brand propagation cases to assist in the development of practical intuition. These brand propagation results, with a Baum-McCaffrey lofting plume, suggest that there is a limiting maximum loftable initial diameter, $D_o^* = 6$. In dimensional terms,

$$d_{o,max} = 6\left(\frac{3C_d}{4}\right)\left(\frac{\rho_a}{\rho_s}\right)\left(\frac{\dot{Q}_o}{\rho_a c_p T_o \sqrt{g}}\right)^{2/5} = 0.454(\beta)(\dot{Q}_o)^{0.4} \quad (28)$$

where the symbols are defined in the notation, $C_d = 0.45$, and β is a correction factor, shown in Table 2. Cedar spheres ($\rho_s = 315$ kg/m^3) will be used for the dimensional examples of this section. For a 1 MW fire ($\Phi = \Phi_1 = 20$), $d_{o,max} = 7.2$ mm; for a 50 MW fire ($\Phi = \Phi_2 = 200$), $d_{o,max} = 34$ mm; and for a 1 GW fire ($\Phi = \Phi_3 = 1100$), $d_{o,max} = 0.11$ m. (See Fig. 11.) These are the heat-release rates for a small pool fire, a fully-involved house fire, and the early stages of the Oakland Hills' Fire of 1991. Using cedar as a reference wood, Φ can be determined from Eq. (21) for a variety of wood types,

$$\Phi = 0.28\beta\dot{Q}_o^{3/5} \quad (29)$$

The "collapse" diameter, above which all diameters have the same propagation distance, can be calculated from

$$D_{col}^* = 4.87\Phi^{-0.218} \quad (30)$$

to within 3% of values calculated from simultaneous solution of Eqs. (19, 20, and 22) for $20 < \Phi < 2100$. In dimensional terms, this translates to

$$d_{col} = 0.49\dot{Q}_o^{0.269}\beta^{0.782} \quad (31)$$

where d_{col} is in mm and $\dot{Q}_o$ is in kW. $\dot{Q}_o < 3$ GW for all applicable dimensional equations in this section. For the three fires above, $d_{col} = 3.1$ mm, 9.0 mm, and 20 mm, respectively. See Fig. 11.

For $D_o^* \geq D_{col}^*$, the maximum dimensionless lofting height is only a function of Φ. The data fits the equation,

$$z_{max,loft}^* = 8.88\Phi^{0.36} \quad (32)$$

This formula, valid to within 2% for $20 < \Phi < 2100$ and $D_o^* \geq D_{col}^*$, is more accurate than that given by Eq. (26) for the specified diameters. For cedar spheres, the maximum lofting height is

$$z_{max,loft} = 0.34\dot{Q}_o^{0.616}\beta^{0.36} \quad (33)$$

where $z_{max,loft}$ is in meters. For the three fires above, $z_{max,loft} = 24$ m, 270 m and 1700 m.

Similarly, the maximum dimensionless propagation height for $D_o^* \geq D_{col}^*$ fits

$$z_{max,prop}^* = 0.56\Phi^{0.388} \quad (34)$$

which is valid to within 7.5% for $20 < \Phi < 2100$,

Table 2. Correlation Factors for Φ

Wood Type	Density (kg/m^3)	β	Wood Type	Density (kg/m^3)	β
Ash, white	638	0.49	Maple, silver	506	0.62
Birch, yellow	668	0.47	Oak, chestnut	674	0.47
Cedar, eastern red	492	0.64	Oak, live	977	0.32
Cedar, northern white	315	1.00	Oak, white	710	0.44
Cherry, wild red	425	0.74	Pine, eastern white	373	0.84
Douglas Fir (coast)	512	0.62	Pine, pitch	542	0.58
Elm, American	554	0.57	Poplar, yellow	427	0.74
Fir, silver	415	0.76	Spruce, white	431	0.73
Ironwood, black	1077	0.29	Walnut, black	562	0.56

$U_w^* < 6$, and $D_o^* \geq D_{col}^*$, and thus is more accurate than Eq. (27) for the specified diameters. For cedar spheres, the maximum propagation height is

$$z_{max,prop} = 0.20\dot{Q}_o^{0.633}\beta^{0.388} \tag{35}$$

where $z_{max,prop}$ is in meters. For the three fires above, $z_{max,prop}$ = 16 m, 190 m and 1300 m. The equation is valid for constant $U_w < 4.62\ \dot{Q}_o^{1/5}$, where U_w is in m/s. $U_w < 18$ m/s, 40 m/s and 73 m/s for the three cases examined in this section.

Figure 9 suggests the following fit to the maximum dimensionless propagation distance as a function of dimensionless wind velocity and burning parameter:

$$\frac{x_{max}^*}{U_w^*} = 4.7\gamma\Phi^{0.42} \tag{36}$$

where

$$\gamma = \frac{0.034\Phi^{0.28} - 0.14}{U_w^*} + U_w^{*-0.05} \qquad 0.3 \leq U_w^* \leq 3$$
$$\gamma = 1 \qquad 3 < U_w^* \leq 6 \tag{37}$$

In the range $20 < \Phi < 2100$, these fits are accurate to within 5% for $0.3 \leq U_w^* \leq 3$ and within 7% for $3 < U_w^* \leq 6$, and enable quick calculation of the maximum dimensionless propagation distance without simultaneously solving Eqs. (19, 20, and 22) over $0 \leq t^* \leq t_b^*$. In dimensional terms,

$$\frac{x_{max}}{U_w} = 0.216G\dot{Q}_o^{0.452}\beta^{0.42} \tag{38}$$

where

$$G = \frac{0.051\beta^{0.452}\dot{Q}_o^{0.471} - 0.108\dot{Q}_o^{0.2}}{U_w} + \frac{0.987\dot{Q}_o^{0.01}}{U_w^{0.05}}$$
$$\text{for} \quad 0.46 \leq \frac{U_w}{\dot{Q}_o^{0.2}} \leq 2.32$$
$$G = 1$$
$$\text{for} \quad 2.32 < \frac{U_w}{\dot{Q}_o^{0.2}} \leq 4.64 \tag{39}$$

With U_w = 10 m/s, Eq. (38) gives x_{max} = 49 m, 290 m and 1100 m for cedar spheres launched above fires with respective heat release rates of 1 MW, 50 MW, and 1 GW. Figure 12 shows the maximum propagation distance, x_{max}, as a function of $\dot{Q}_o$, parameterized in horizontal wind, where the propagation distance increases parabolically with $\dot{Q}_o$. Figure 13 shows x_{max} as a function of horizontal wind, parameterized in $\dot{Q}_o$. The variation in the ranges of U_w for each $\dot{Q}_o$ results from the limits on U_w^*, where $0.3 \leq U_w^* \leq 6$ for this study.

Conclusions

Brand momentum conservation was used to determine the maximum propagation distances of spherical wooden brands lofted above an axisymmetric pool fire in a constant, horizontal wind.[6] Brand diameters were assumed to decrease in the manner of burning liquid fuel droplets. Simultaneous solution of equations was performed on brand velocity and position equations in the horizontal and vertical directions, along with diameter regression rate, for a range of dimensionless initial diameters ($0 \leq D_o^* \leq 6$),

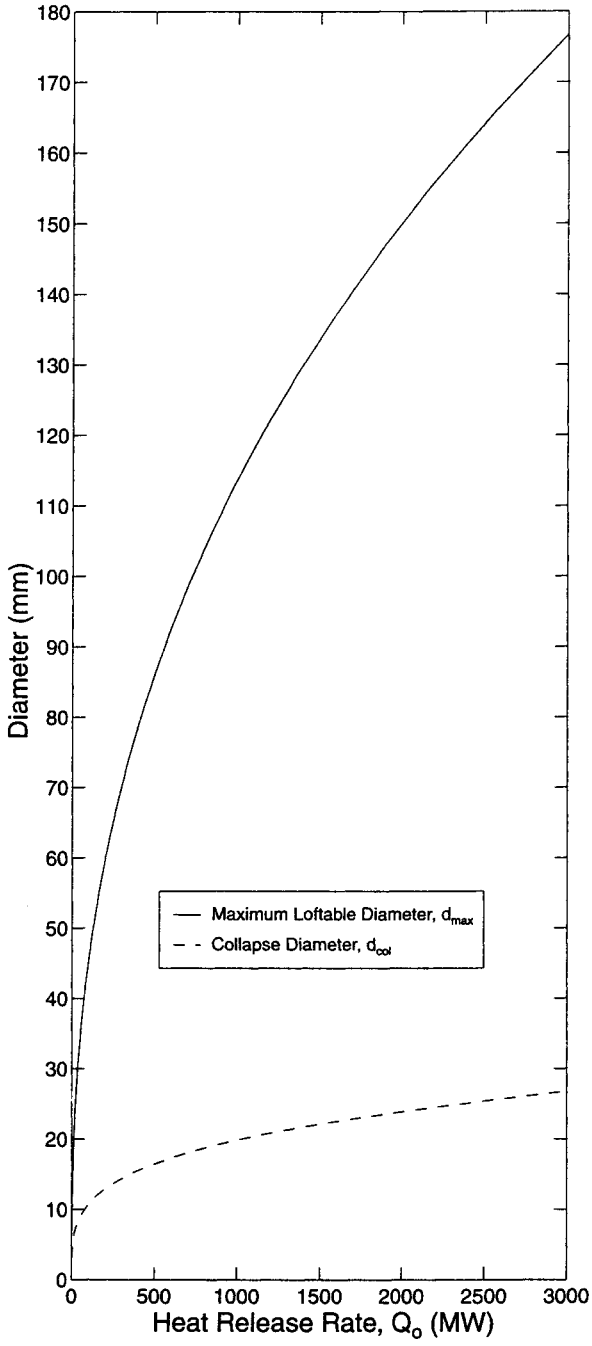

Figure 11. Maximum loftable diameter and collapse diameter as a function of heat release rate for cedar spheres.

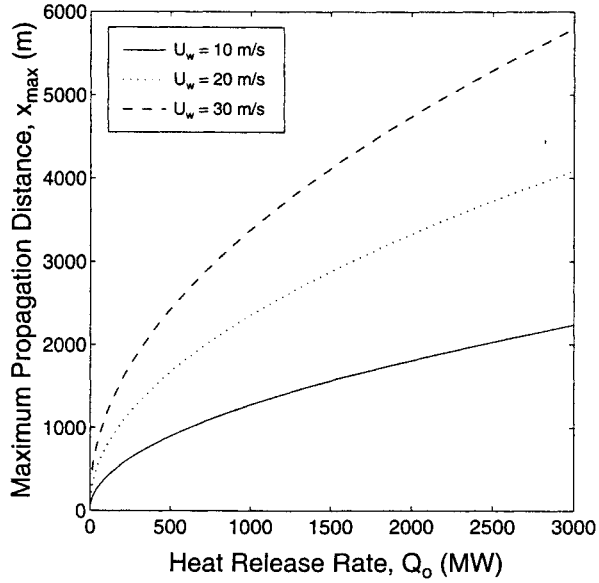

Figure 12. Maximum propagation distance as a function of heat release rate for cedar spheres in ambient wind as noted. The initial diameter of lofted spheres for a given $\dot{Q}_0$ is greater than or equal to the corresponding collapse diameter.

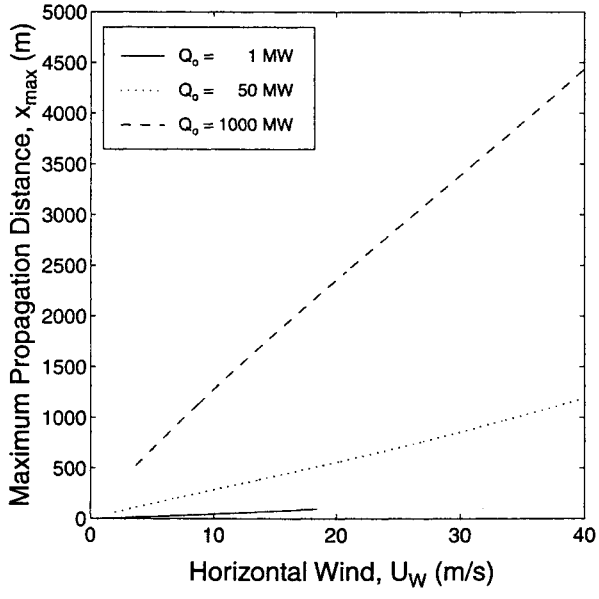

Figure 13. Maximum propagation distance as a function of horizontal wind for as noted. Due to range of dimensionless horizontal wind studied, $0.3 < U_w^* < 6$, minimum velocity increases with $\dot{Q}_0$ (U_w = fn($\dot{Q}_0$))

burning parameters ($20 \leq \Phi \leq 2100$), and ambient winds ($0.3 < U_w^* < 6$). These dimensionless results were also presented in dimensional form for cedar brands, along with correction factors for other wood types.

Future work will implement an improved burning model incorporating forced-flow combustion for multiple brand shapes. Experiments in a low-speed combustion wind tunnel are currently underway to determine combustion models for disk-shaped and cylindrical brands. These burning brands will be inserted as Lagrangian particles in large eddy simulation models, developed at NIST by McGrattan, Rehm, and Baum[23-26] to describe the interaction of the flow field above

large fires with complex terrain and ambient winds. The effects of brand size and shape distributions will be incorporated.

Acknowledgments

We are grateful for the financial support provided by the Building and Fire Research Laboratory of the National Institute of Standards and Technology, U.S. D.O.C., under Grant No. 60NANB3D1438, and by a student grant from the Educational and Scientific Foundation of the Society of Fire Protection Engineers.

Notation

A_c	Cross-sectional area (m^2)
B	Mass transfer number
c_p	Specific heat of air (J/kg K)
C_d	Coefficient of drag
d	Diameter (m)
D	Dimensionless diameter
F	Force (N)
g	Gravity (m/s^2)
G	Modifier for Eq. (38)
$\hat{\mathbf{k}}$	Unit vector in z-direction
m	Particle mass (kg)
$\dot{Q}_o$	Rate of heat release for the fire (kW)
Re	Reynolds Number
t	Time (s)
T_o	Ambient temperature (K)
U	Velocity of surroundings (m/s)
V	Vector-valued particle velocity relative to ground (m/s)
V	Scalar particle velocity relative to ground (m/s)
W	Vector-valued relative velocity of brand to its surroundings (m/s)
W	Scalar relative velocity of brand to its surroundings (m/s)
z	Vertical height of particle (m)

Greek

α	Thermal diffusivity of air (m^2/s)
β	Correction factor for wood
γ	Modifier for Eq. (36)
ν	Kinematic viscosity of air (m^2/s)
ρ	Density (kg/m^3)
Φ	Droplet parameter

Superscript

*	Dimensionless variable

Subscripts

a	Air
b	Burn-out
c	Characteristic constant
d	Drag
g	Gravity
loft	Lofting
max	Maximum
o	Initial
p	Plume
prop	Propagation
s	Sphere
w	Ambient Wind
x, y, z	Cartesian coordinate direction

References

1. Pagni, P.J., "Causes of the 20 October 1991 Oakland Hills Conflagration," *Fire Safety Journal*, Vol. 21, No. 4, 1993, pp. 331–340.

2. Muraszew, A., "Firebrand Phenomena," *Aerospace Report No. ATR-74 (8165-01)-1*, The Aerospace Corporation, El Segundo, CA, 1974.

3. Muraszew, A. and Fedele, J.B., "Statistical Model for Spot Fire Hazard," *Aerospace Report No. ATR-77 (7588)-1*, The Aerospace Corporation, El Segundo, CA, 1976.

4. Albini, F.A., "Spot Fire Distance From Burning Trees: A Predictive Model," *General Technical Report No. INT-56*, USDA Forest Service Intermountain Forest and Range Experiment Station, Ogden, UT, 1979.

5. Albini, F.A., "Transport of Firebrands by Line Thermals," *Combustion Science and Technology*, Vol. 32, 1983, pp. 277–288.

6. Woycheese, J.P., Pagni, P.J. and Liepmann, D, "Brand Lofting Above Large-Scale Fires," *Proceedings of the Second International Conference of Fire Research and Engineering*, Society of Fire Protection Engineers, 1998, pp. 137–150.

7. Tarifa, C.S., del Notario, P.P. and Moreno, F.G., "On the Flight Paths and Lifetimes of Burning Particles of Wood," *Tenth Symposium (International) on Combustion*, The

Combustion Institute, Pittsburgh, PA, 1965, pp. 1021–1037.

8. Tarifa, C.S., del Notario, P.P., Moreno, F.G. and Villa, A.R., "Transport and Combustion of Firebrands," *Final Report of Grants FG-SP-114 and FG-SP-146*, Vol. 2, USDA, Madrid, 1967.

9. Lee, S.-L. and Hellman, J.M., "Firebrand Trajectory Study Using an Empirical Velocity-Dependent Burning Law," *Combustion and Flame*, Vol. 15, No. 3, 1970, pp. 265–274.

10. Lee, S.-L. and Hellman, J.M., "Study of Firebrand Trajectories in a Turbulent Swirling Natural Convection Plume," *Combustion and Flame*, Vol. 13, No. 6, 1969, pp. 645–655.

11. Baum, H.R. and McCaffrey, B.J., "Fire Induced Flow Field – Theory and Experiment," *Fire Safety Science, Proceedings of the Second International Symposium*, ed. T. Wakamatsu et al., Hemisphere, Washington, DC, 1989, pp. 129–148.

12. Taylor, G.I., "Notes on Possible Equipment and Techniques for Experiments on Icing of Aircraft," *Journal of Aerospace Sciences*, Vol. 25, 1958, p. 464.

13. Woycheese, J.P., "Brand Lofting in Large Scale Fires," *M.S. Thesis*, University of California, Berkeley, 1996.

14. Zukoski, E.E., "Fluid Dynamic Aspects of Room Fire," *Fire Safety Science, Proceedings of the First International Symposium*, ed. Cecil Grant and P.J. Pagni, Hemisphere, Washington, DC, 1986, pp. 1–30.

15. McCaffrey, B.J., "Momentum Implications for Buoyant Diffusion Flames," *Combustion and Flame*, Vol. 52, 1983, pp. 149–167.

16. Trelles, J. and Pagni, P.J., "Fire-Induced Winds in the 20 October 1991 Oakland Hills Fire," *Fire Safety Science, Proceedings of the 5th International Symposium*, IAFSS, Boston, MA, 1997, pp. 911–922.

17. Davis, K.P., *Forest Fire – Control and Use*, McGraw-Hill, New York, NY, 1959.

18. Clift, R., Grace, J.R. and Weber, M.E., *Bubbles, Drops, and Particles*, Academic Press, New York, NY, 1978.

19. Flemmer, R.L.C. and Banks, C.L., "On the Drag Coefficient of a Sphere," *Powder Technology*, Vol. 48, No. 3, 1986, pp. 217–221.

20. Turton, R. and Levenspiel, O., "A Short Note on the Drag Correlation for Spheres," *Powder Technology*, Vol. 47, 1986, pp. 83–86.

21. Haider, A. and Levenspiel, O., "Drag Coefficient and Terminal Velocity of Spherical and Nonspherical Particles," *Powder Technology*, Vol. 58, 1989, pp. 63–70.

22. Pagni, P.J., "Diffusion Flame Analyses," *Fire Safety Journal*, Vol. 3, 1980/81, pp. 273–285.

23. McGrattan, K.B., Ferek, R.J. and Uthe, E.E., "Smoke Plume Trajectory from In Situ Burning of Crude Oil—Field Experiments," *Proceedings of the International Conference on Fire Research and Engineering*, ed. D. Peter Lund, Society of Fire Protection Engineers, Orlando, FL, 1995, pp. 47–52.

24. McGrattan, K.B., Rehm, R.G., Tang, H.C. and Baum, H.R., "A Boussinesq Algorithm for Buoyant Convection in Polygonal Domains," *NISTIR 4831*, National Institute of Standards and Technology, Gaithersburg, MD, 1992.

25. McGrattan, K.B., Baum, H.R. and Rehm, R.G., "Smoke Plumes from Large Fires," *UJNR Panel on Fire Research*, UJNR, Gaithersburg, MD, 1995.

26. McGrattan, K.B., Baum, H.R., Walton, W.D. and Trelles, J., "Smoke Plume Trajectory from In Situ Burning of Crude Oil in Alaska – Field Experiments and Modeling of Complex Terrain," *NISTIR 5958*, NIST, Gaithersburg, MD, 1997.